Virtual Sensors for Diesel Engines

To enable efficient operation while simultaneously producing low levels of exhaust emissions, modern passenger car diesel engines have significantly increased their degrees of freedom in operation. A feed forward and feedback control of emissions would ensure the operation of the complex system always at its optimum. In a FVV research project, model-based virtual emission sensors were derived at the ETH Zurich, provide the information faster (even before the combustion event) and cheaper than physical sensors, while being more robust in long term operation. These sensors can be used for model based feedforward control and can be integrated into a feedback control loop. The test bench measurements showed that the virtual sensors are able to predict transient emissions and could replace physical sensors.

AUTHORS

Dr. Christophe Barro is Senior Research Associate at the Aerothermochemistry and Combustion Systems Laboratory (LAV) at the ETH Zurich and co-founder of Vir2sense GmbH (Switzerland).

Prof. Dr. Konstantinos Boulouchos is Head of the Aerothermochemistry and Combustion Systems Laboratory (LAV) at the ETH Zurich (Switzerland).

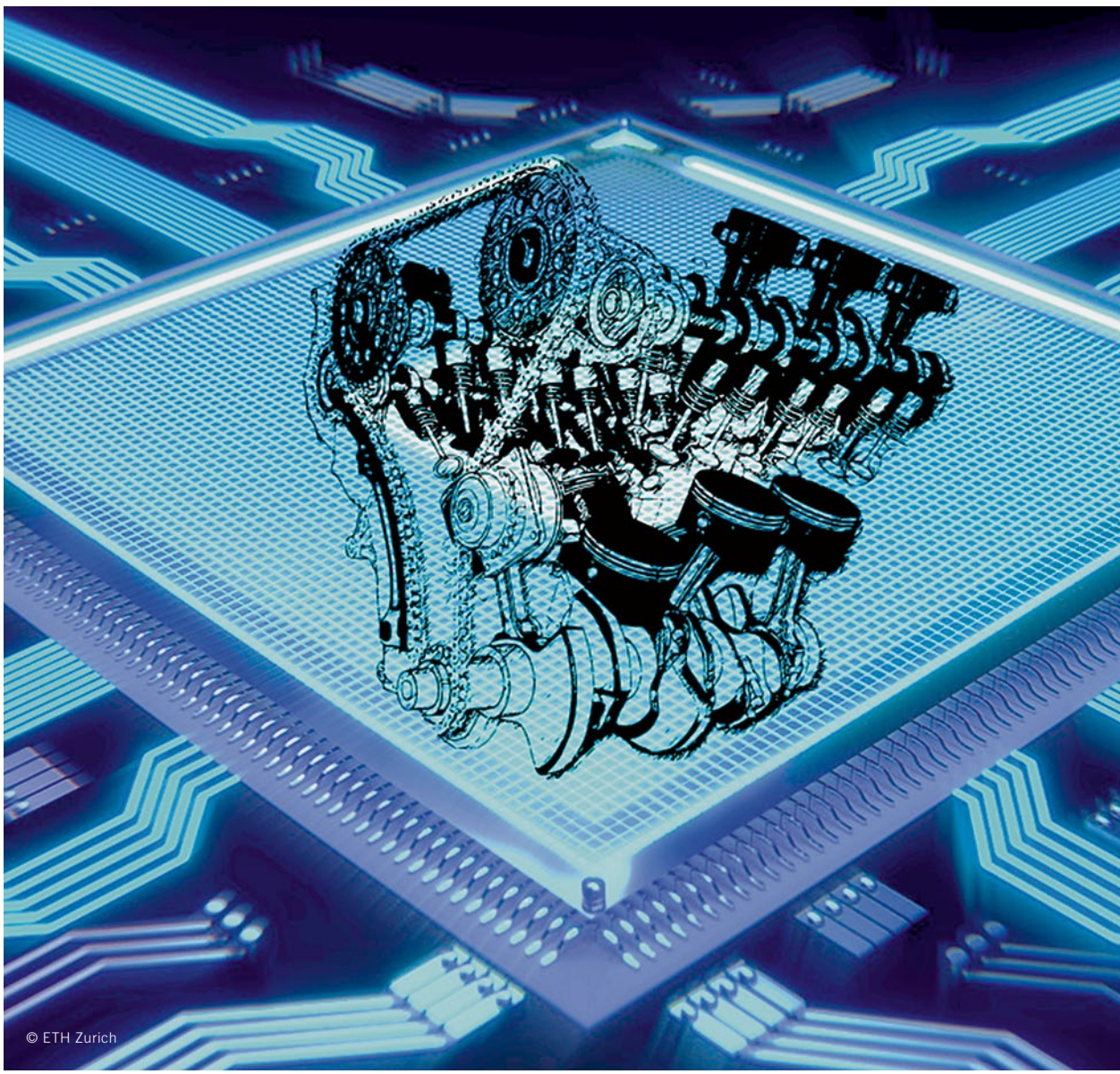

1 MOTIVATION

Future emission legislation for diesel engines will be increasingly challenging to fulfil, in particular for real driving conditions. For control and monitoring of the exhaust gas aftertreatment system and for feedback control of the emissions, emission sensors are required. The operation of physical sensors in the hot and toxic environment of an exhaust pipe requires the use of costly sensors which will offer the necessary robustness. Furthermore, in case of physical sensors, it is only possible to measure emissions in the exhaust pipe rather than in the cylinder, which introduces a necessary time delay with respect to the cycle when they have been formed.

The abovementioned issues can be solved with the development of virtual sensors – this are physically consistent phenomenological models, which accurately describe the emission formation depending on all relevant influencing parameters. The model description needs to be significantly simplified, so that the calculation can be performed online on an ECU. Contrary to empirical, "black box" models, the modelling approach which captures the physical processes allows the model to be extrapolated to operating conditions outside of the calibrated range. Several examples can be found in the literature where the reduction of the spatial [1, 2] and the temporal dimensions [3] lead to the development of so called mean value models, which match the compromise between accuracy and calculation time.

In [4], a virtual soot sensor has been developed providing the signal for soot emission feedback control. In this case however acquired direct cylinder pressure has been used as a model input. In this work, the input of the virtual soot sensor and a newly developed virtual NO_x sensor comes from a virtual pressure sensor, which contains a heat release model. This step is required to enable model based feedforward control.

2 MODELLING

As already mentioned, since the measured cylinder pressure is not available, the inputs for the emission models need to be provided by a heat release model, which reproduces the process of combustion.

2.1 HEAT RELEASE RATE MODEL

The heat release rate (solid line in **FIGURE 1**; engine: Daimler OM 642 with 3 l displacement volume) shows that a typical combustion process can roughly be divided into 3 different parts: the pilot combustion, the fuel injection controlled diffusion combustion and the late phase combustion. The heat release rate model approximates each of these phases with a vibe function of the type:

$$\textbf{Eq. 1} \quad \frac{dQ}{d\varphi} \approx k \cdot (-a) \cdot (m_v + 1) \cdot \left(\frac{\varphi}{\Delta\varphi_v}\right)^{m_v} \cdot \exp\left\{a \cdot \left(\frac{\varphi}{\Delta\varphi_v}\right)^{(m_v+1)}\right\}$$

The variable φ represents the crank angle degree after firing top dead center. Q represents the total amount of heat released during the combustion phase. Superimposing the three vibe functions with the corresponding parameters, **FIGURE 1**, reproduces the measured heat release rate. Each of the vibe functions contains three parameters: the factor $\Delta\varphi_v$ describes the spread in the crank angle direction (duration of combustion), the exponent m_v defines the form of the function ($m_v = 2$ results in a symmetric form, $m_v < 2$ shifts the maximum towards left) and k scales the whole form. The factor a is fixed at -6.9 l/°CA for complete combustion according to [5].

This model has been developed for operating conditions with pilot injection application. Using pilot injection decreases the ignition delay of the main injection, thus the premixed portion decreases to a negligible value. For operation without pilot injection, the model needs to be adjusted to include a premixed combustion portion and a coupling of premixed and diffusion combustion.

The description of the pilot combustion is simplified considerably. The form $m_{v,PI} = 2$ is symmetric and the duration is constant $\Delta\varphi_{v,PI} = 8$ °CA. In most cases the portion of pilot fuel is small in comparison to the main injection; this limits the error arising from this simplification. The scale factor k is proportional to pilot fuel quantity.

$$\textbf{Eq. 2} \quad k_{PI} = \left(\frac{m_{f,PI}}{m_{f,TOT}}\right) - \left(\frac{m_{f,U}}{m_{f,TOT}}\right)$$

The first term depends on the pilot fuel quantity $m_{f,PI}$ as a portion of the total fuel quantity $m_{f,TOT}$ in grams per cycle and cylinder. The second term considers that occasionally part of the fuel introduced in the pilot injection is not combusted during the pilot combustion. The unburned portion $m_{f,U}$ scales linearly with the ignition delay $\Delta\varphi_{ID}$:

$$\textbf{Eq. 3} \quad \left(\frac{m_{f,U}}{m_{f,TOT}}\right) \approx p_{PI} \cdot \left(\frac{\Delta\varphi_{ID}}{\Delta\varphi_{ID,ref}}\right)$$

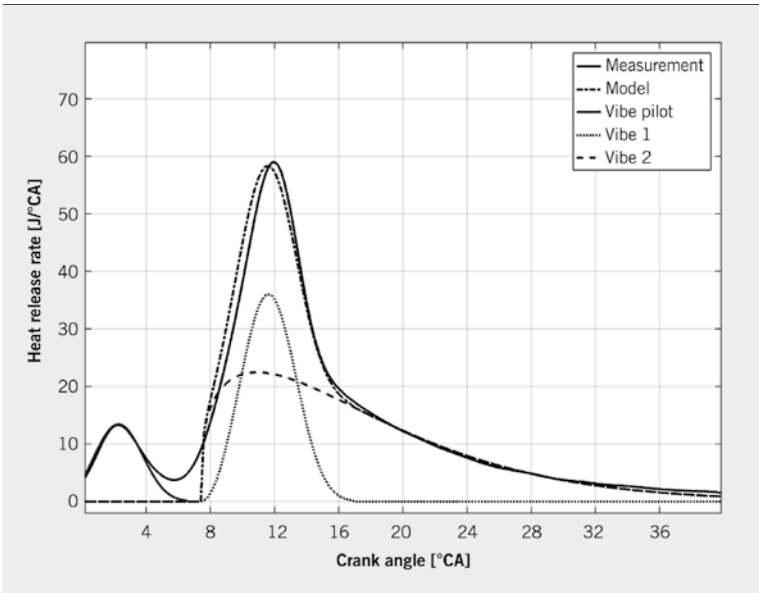

FIGURE 1 Heat release rate calculated from the measured cylinder pressure (solid), modelled heat release rate (dashed and dotted), three vibe functions for pilot combustion (grey, bolt) and main combustion (dotted and dashed) (© ETH Zurich)

The ignition delay model of Hardenberg and Hase [6] is used. The reference ignition delay is set to $\Delta\varphi_{ID,ref}$ = 1°. The diffusion combustion of the main injection is divided in two parts. The first of the parts, the fuel controlled part uses a constant form factor $m_{v,1}$ = 1.6. This results in a nearly symmetric function. Furthermore, the duration of combustion is set to twice the duration of injection:

Eq. 4 $$\Delta\varphi_{v,1} = 2 \cdot \Delta\varphi_{MI}$$

The maximum of the fuel controlled combustion is therefore at the end of injection. The scaling factors k_1 and k_2 are determined as a sum

Eq. 5 $$k = k_1 + k_2$$

with the total energy balance

Eq. 6 $$m_{f,MI} \cdot H_u = Q_1 + Q_2$$

where the fuel mass multiplied with the lower heating value (left hand side) must balance the energy coming from the integration of the vibe functions of the main combustion (right hand side). The weight of each scaling factor is described using

Eq. 7 $$k_1 = k \cdot (1 - \zeta)$$

Eq. 8 $$k_2 = k \cdot \zeta$$

where ζ is the weighting factor between the fuel injection controlled and the late phase combustion. The weighting factor depends on the main injection fuel quantity, swirl valve position u_{EKAS}, stoichiometric EGR ratio x_{BG} and the unburned fuel portion from the pilot injection:

Eq. 9 $$\zeta \approx 0.6 + p_1 \cdot \left(\frac{m_{f,MI}}{m_{f,MI,ref}}\right) + p_2 \cdot \left(\frac{u_{EKAS}}{u_{EKAS,ref}}\right) + p_3 \cdot x_{BG} + p_4 \cdot \left(\frac{m_{f,U}}{m_{f,TOT}}\right)$$

The following reference values have been set: the main injection fuel mass

Eq. 10 $$m_{f,MI,ref} = 1 \frac{g}{Cyl.\ cycle}$$

and swirl valve position

Eq. 11 $$u_{EKAS,ref} = 100\,\%$$

The modelling of the late phase combustion includes the global oxygen availability (using the stoichiometric EGR ratio) and the background turbulence (using the engine speed n and the swirl valve position u_{EKAS}. The form factors for the vibe function for the burn-out were modeled as follows:

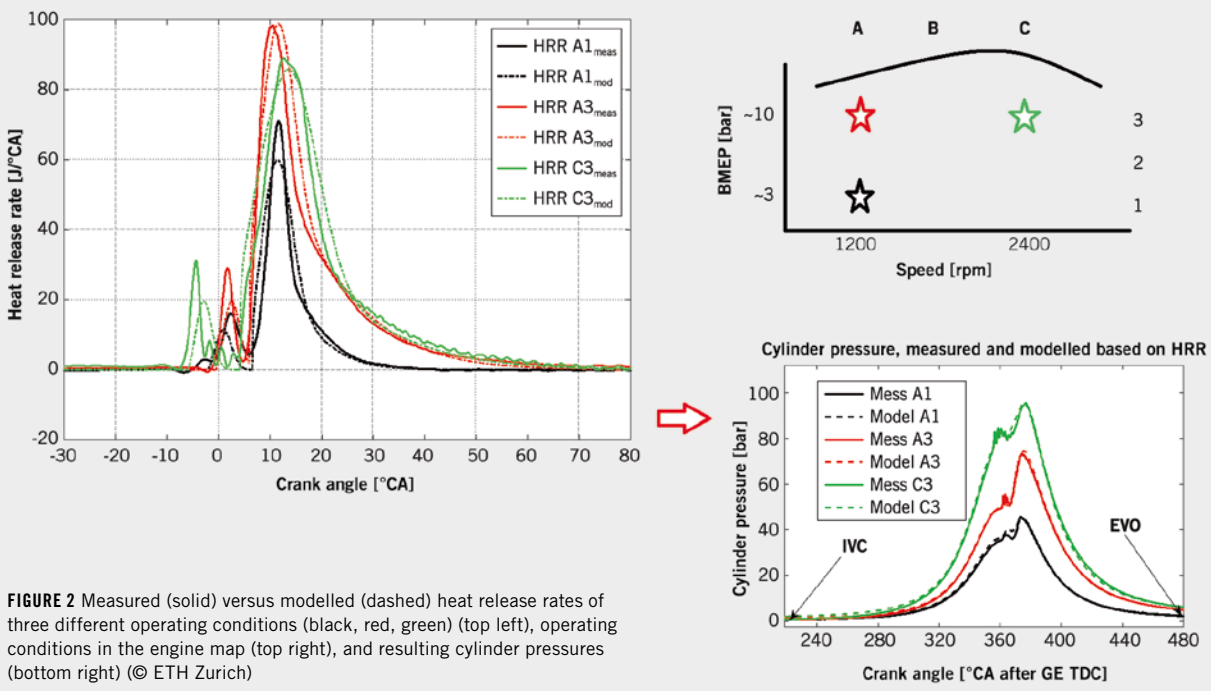

FIGURE 2 Measured (solid) versus modelled (dashed) heat release rates of three different operating conditions (black, red, green) (top left), operating conditions in the engine map (top right), and resulting cylinder pressures (bottom right) (© ETH Zurich)

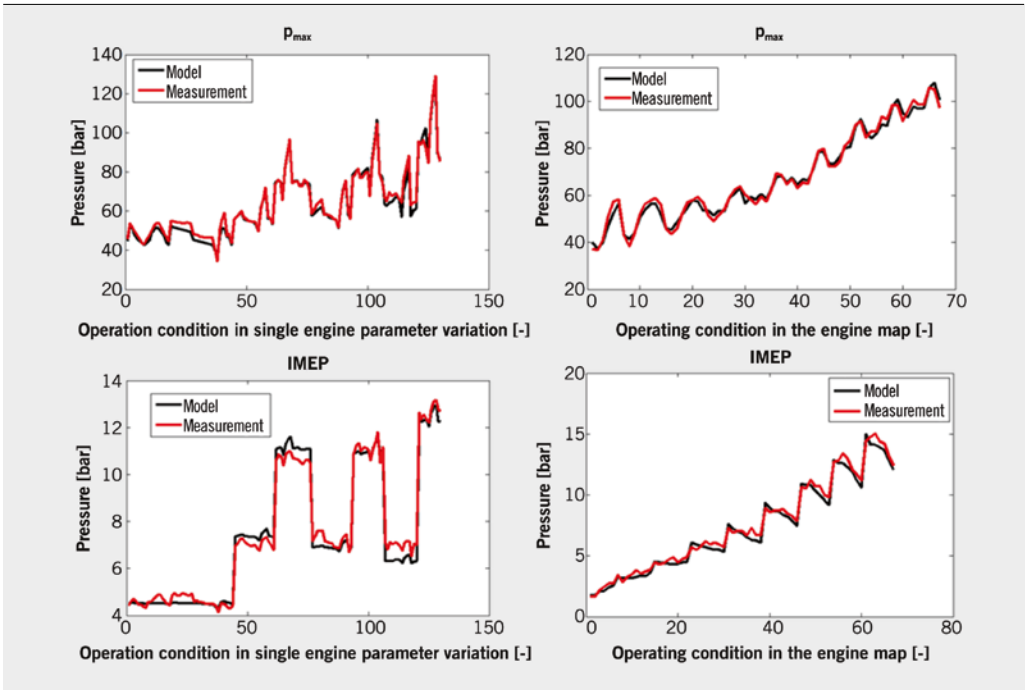

FIGURE 3 Combustion characteristics of measured (red) and modelled (black) cylinder pressures (© ETH Zurich)

$$\textbf{Eq. 12}\quad m_{v,2} = 0.3 - p_5 \cdot \left(\frac{m_{f,MI}}{m_{f,MI,ref}}\right) + p_6 \cdot \left(\frac{n}{n_{ref}}\right) + p_7 \cdot \left(\frac{u_{EKAS}}{u_{EKAS,ref}}\right)$$

$$\textbf{Eq. 13}\quad \varphi_{v,2} = 30° + p_8 \cdot \left(\frac{m_{f,MI}}{m_{f,MI,ref}}\right) \cdot 1° + p_9 \cdot \left(\frac{u_{EKAS}}{u_{EKAS,ref}}\right) \cdot 1° + p_{10} \cdot x_{BG} \cdot 1° + p_{11} \cdot (u_{SOI} + 4°)$$

Here the reference speed is set to n_{ref} = 1000 rpm. The model parameters p_{PI} and p_1 to p_{11} need to be calibrated. In this particular case the calibration of the parameters has been performed using seven different load conditions with variations of u_{EKAS}, u_{AGR} and u_{SOI}, to create a total of 130 operating conditions. **FIGURE 2** (left) shows a comparison of the modelled and measured (calculated using the measured pressure curve) heat release rate, for three different operating conditions in the engine map, **FIGURE 2** (top right). Using the first law approach, a modelled cylinder pressure has been derived out of the modelled heat release rate (virtual pressure sensor). The comparison with the measurements is visible in **FIGURE 2** (bottom right part).

FIGURE 3 shows the measured (red) and modeled (black) maximum pressure (top) and medium pressure (bottom) for individual parameter variations (left) and over the entire working range (right). There is a good match between model prediction and measurement.

2.2 FORMATION OF NITROUS OXIDES

The model developed here uses a mean, representative NO_x formation rate over the duration of the total burn-out. Since it is assumed that the reaction takes place away from the point of equilibrium, it has been assumed here that the kinetics of the forward reaction can represent the process with sufficient accuracy:

$$\textbf{Eq. 14}\quad \frac{d[NO]^*}{d\varphi} = k^+ \cdot p_{NO,1} \cdot \left(p_{NO,2}\left(1 - x_{BG} \cdot p_{NO,3}\right)\right)^{0.5} \cdot \exp\left\{\frac{E_a}{R \cdot T}\right\}$$

The variable $k^+ = 4.68 \cdot 10^{13}$ °CA^{-1} describes the reaction velocity of the forward reaction. The parameters $p_{NO,2}$ and $p_{NO,3}$ represent the local concentration of oxygen and nitrogen respectively. The parameter $p_{NO,1}$ is a scale parameter and could have been combined with $p_{NO,2}$. The factor $\frac{E_a}{R}$ = -67838 K is the activation energy divided by the gas constant. The nitrous oxide concentration at the end of the combustion is evaluated with the temporal integration of the representative formation rate along the duration of the late phase combustion $\varphi_{v,2}$

$$\textbf{Eq. 15}\quad [NO] = d[NO]^* \cdot \varphi_{v,2} \cdot \frac{V_{NO}}{V_{cyl}}$$

whereas the for the calculation of the representative volume, the ratio of the formation volume and the total cylinder volume at the time $\frac{\varphi_{v,2}}{2}$ is:

$$\textbf{Eq. 16}\quad \frac{V_{NO}}{V_{cyl}} = (1 - \zeta) \cdot \left(\frac{m_f}{m_{f,ref}}\right)^{p_{NO,4}} \cdot \left(\frac{n_{ref}}{n}\right)^{p_{NO,5}} \cdot \left(\frac{p_{IVC}}{p_{amb}}\right)^{p_{NO,6}} \cdot p_{NO,7}$$

The variable p_{IVC} states the cylinder pressure at the time when the intake valves close and p_{amb} ambient pressure. The reference values of fuel mass and engine speed have been set to

$$\textbf{Eq. 17}\quad m_{f,ref} = 1\,\frac{g}{Cyl.\,cycles}$$

and

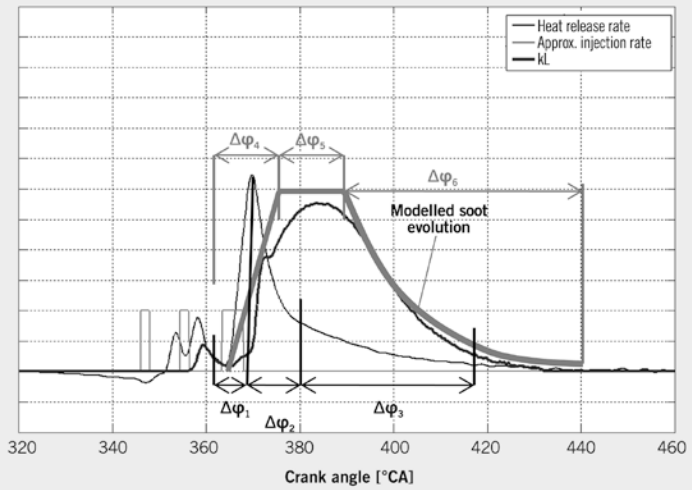

FIGURE 4 Injection profile, heat release rate and measured soot evolution with an according modelled soot evolution including the described phases (schematic representation) [4] (© ETH Zurich)

Eq. 18 $n_{ref} = 1000/min$

The model parameters $p_{NO,1}$ to $p_{NO,7}$ require explicit calibration.

2.3 SOOT FORMATION

The soot model used has already been presented in [4]. In this application it has been adapted to the change in inputs. In the current work the inputs are sourced from the heat release rate model instead of cylinder pressure measurement. **FIGURE 4** shows the concept of the model. The goal of the model is to reproduce the measured soot evolution (kL-evolution, measured using a pyrometer). The evolution is divided in three different phases: a formation dominated phase, an equilibrium phase and an oxidation dominated phase. The duration of the phases depends on characteristic durations of the heat release rate ($\Delta\varphi_{1\text{-}3}$). The formation dominated phase depends mainly on the fuel mass which participates in the diffusion combustion:

Eq. 19 $$m_{PM} = p_{PM,1} \cdot (m_{f,U} + m_{f,MI})^{p_{PM,2}}$$

This is followed by the equilibrium phase, where the soot mass does not change. During the oxidation dominated phase the soot mass is reduced following an exponential function:

Eq. 20 $$m_{PM,end} = m_{PM,init} \cdot (0.01 + \exp\{-B \cdot \Delta\varphi_6\})$$

The duration of this phase is proportional to the duration of the late phase combustion $\Delta\varphi_3$ which can be estimated using the modelled heat release rate

Eq. 21 $$\Delta\varphi_6 \approx \frac{p_{PM,3} \cdot \Delta\varphi_3}{\varphi_{ref}}$$

The exponential factor B considers the influence of the temperature (T_{ox} from the heat release rate), the oxygen availability (using stoichiometric EGR ratio and λ), the turbulence (rail pressure p_{rail}, swirl valve and engine speed) as well as the injected fuel mass

Eq. 22 $$B \approx \left(\frac{T_{ox}}{T_{ref}}\right)^{p_{PM,4}} \cdot (1 + p_{PM,5} x_{BG})^{-p_{PM,6}} \cdot \left(\frac{1}{2} \cdot p_{PM,7} \cdot \lambda\right)^{p_{PM,8}} \cdot \left(\frac{p_{rail}}{p_{rail,ref}}\right)^{p_{PM,9}} \cdot \left(\frac{5}{\sin\left(u_{EKAS}\frac{\pi}{2}\right)}\right)^{p_{PM,10}} \cdot \left(\frac{n}{n_{ref}}\right)^{p_{PM,11}} \cdot m_{f,TOT}^{p_{PM,12}}$$

The reference values for temperature and rail pressure have been set to: T_{ref} = 1600 K and $p_{rail,ref}$ = 1000 bar. The model parameters $p_{PM,1}$ to $p_{PM,12}$ require explicit calibration.

3 VALIDATION OF THE EMISSION MODELS

In order to demonstrate the accuracy and the capability to be extrapolated, the models have been validated in steady state as well as in transient engine operation. For the validation, a different set of operating conditions then for the calibration has been used.

3.1 STEADY STATE VALIDATION

FIGURE 5 shows the correlation of the output of the virtual emission sensors and the measured values in the exhaust. **FIGURE 5** (left) shows the NO_x emissions and the **FIGURE 5** (right) the soot emissions for almost 2000 operating conditions, including some with extreme values for EGR or SOI. The accuracy of the NO_x model is very good barring some extreme conditions. The route mean square error (RMSE) is less than 3 %.

The aforementioned extreme conditions, especially for high EGR ratios, create high volatility in soot emissions since the soot formation and oxidation process is very sensitive to local changes in such conditions. This limits the steady state accuracy of the soot model for high soot emission levels. However, the RMSE is less than 6 %.

3.2 DYNAMIC VALIDATION

For the validation under dynamic conditions, the virtual sensors

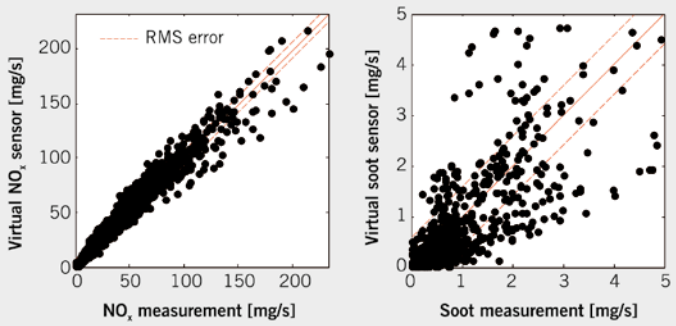

FIGURE 5 Correlation of model output (y-axis) and exhaust measurement (x-axis) for NO_x (left) and soot (right) (© ETH Zurich)

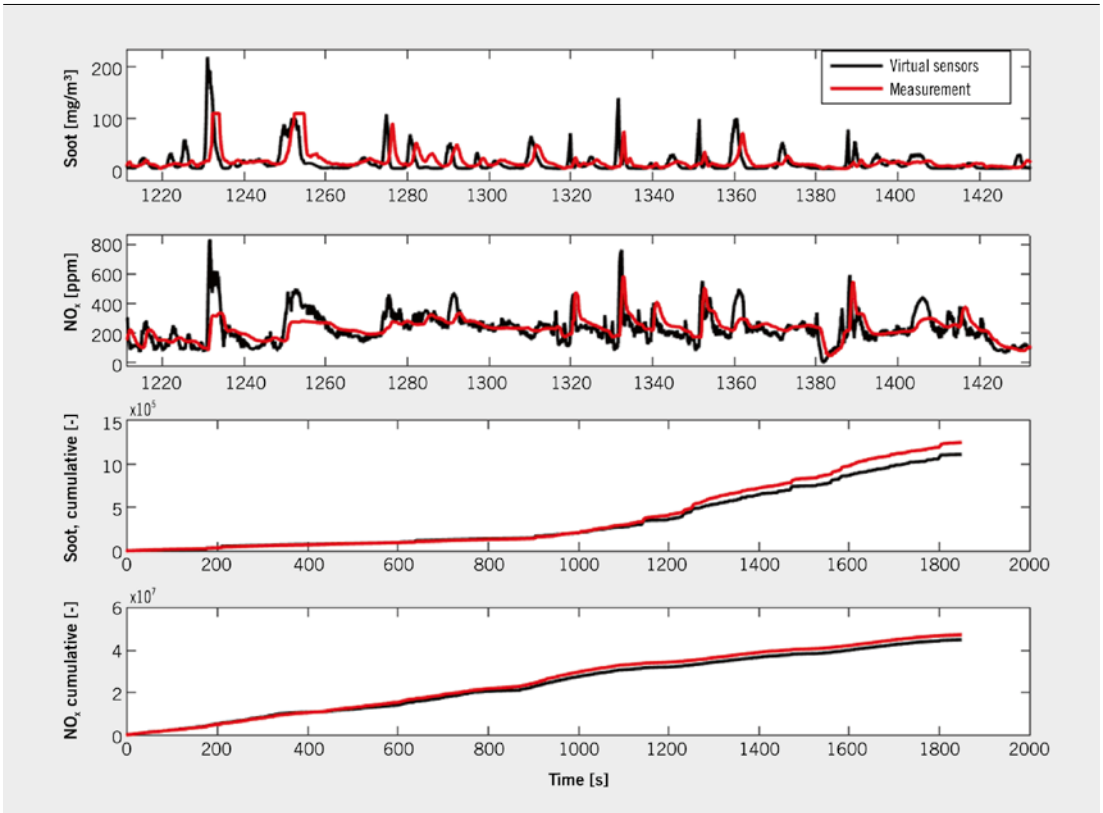

FIGURE 6 Comparison of the measured (red) and estimated (black) soot and NO_x emissions (the top two graphs show a section of the WLTP, the bottom two graphs the cumulative values of the entire WLTP) (© ETH Zurich)

have been implemented on a ECU and evaluated online during engine operation. **FIGURE 6** shows the measured (red) and modelled traces of soot, **FIGURE 6** (top), and NO_x, **FIGURE 6** (second graph from top), for a section of the WLTP cycle. It is visible, that the virtual sensors predict accurate values during accelerations. Furthermore, the time the values of the virtual sensors are approximately one second before the measurements and even before the cycle of interest available. **FIGURE 6** (third and fourth graph) shows the values of the soot (third graph) and nitrogen oxide emissions (fourth graph) accumulated over the entire duration of the driving cycle. It can be seen that model predictions of the virtual sensors correlate well with reality.

4 SUMMARY AND OUTLOOK

Modern diesel engines offer a variety of actuators, which are used to influence the raw emissions of the engine. The application of the control units is a time-consuming and labor-intensive step of the overall process. Conventional, intuitive methods are not useful. Virtual sensors can be used to optimize the calibration and control of emissions. This work provides insights about newly developed virtual emission sensors, providing the information faster and cheaper than physical sensors while increasing their reliability. These models can be used for model based feedforward control and integration into a feedback control loop. The test bench measurements showed that the virtual sensors are able to predict transient emissions and could replace physical sensors.

In future research the virtual sensors will be used to allow the ECU calibration using a model based optimization (virtual test bench), which allows the reduction of complex and costly test bench time. In addition, investigations towards adaptations of the virtual sensors to allow the modelling of cold starts are ongoing.

REFERENCES

[1] Schubiger, R.; Boulouchos, K.; Eberle, M.: Rußbildung und Oxidation bei der dieselmotorischen Verbrennung. In: MTZ 63 (2002), No. 5, pp. 342–353
[2] Warth, M.: Vorausberechnung von Brennverlauf, NO- und Rußemissionen beim Dieselmotoroptimierung und Validierung eines neuen Ansatzes. 9. Tagung Arbeitsprozess des Verbrennungsmotors, Graz, 2003
[3] Kirchen, P.; Boulouchos, K.: A Phenomenological Mean Value Soot Model for Transient Engine Operation. In: MTZworldwide 69 (2008), No. 7–8, pp. 58–65
[4] Barro, C.; et al.: Development of a Virtual Soot Sensor in Diesel Engines. In: MTZworldwide 75 (2014), No. 6, pp. 42–49
[5] Vibe, I. I.: Brennverlauf und Kreisprozess von Verbrennungsmotoren. Berlin: VEB Verlag Technik, 1970
[6] Heywood, J. B.: Internal combustion engine fundamentals. New York: McGraw-Hill, 1988

THANKS

The FVV-project no. 1140 Emission Optimized Diesel Engine has been supported by the FVV and by the Swiss Federal Office of Energy. The authors would like to thank the supporting organizations for enabling this project. Furthermore, we would like to thank the FVV research group with the other chairmen Pedro Macri-Lassus (Daimler AG). Further the authors would like to thank Dr. Philipp Elbert and Dr. Alois Amstutz from the Institute for Dynamic Systems and Control of ETH Zurich.